

Automated and Robust Quantification of Colocalization in Dual-Color Fluorescence Microscopy: A Nonparametric Statistical Approach

Shulei Wang^{*,†}, Ellen T. Arena^{†,‡}, Kevin W. Eliceiri^{†,‡}, and Ming Yuan^{*,†,‡,§}

Abstract—Colocalization is a powerful tool to study the interactions between fluorescently labeled molecules in biological fluorescence microscopy. However, existing techniques for colocalization analysis have not undergone continued development especially in regards to robust statistical support. In this paper, we examine two of the most popular quantification techniques for colocalization and argue that they could be improved upon using ideas from nonparametric statistics and scan statistics. In particular, we propose a new colocalization metric that is robust, easily implementable, and optimal in a rigorous statistical testing framework. Application to several benchmark datasets, as well as biological examples, further demonstrates the usefulness of the proposed technique.

Index Terms—colocalization, fluorescence microscopy, hypothesis testing, nonparametric statistics, scan statistics.

I. INTRODUCTION

COLOCALIZATION is a powerful tool in examining macromolecules' spatial relationships to other macromolecules and cellular features. The goal of colocalization is to quantify the co-occurrence and/or correlation between two fluorescently-labeled molecules. Colocalization via fluorescence microscopy can yield quantitative, correlative spatiotemporal information. Yet historically, it has been often conducted in a rather ad hoc fashion, primarily through visual inspection of the overlaid microscopic images for both fluorescent signals; when two molecules of interest are labeled in “red” and “green”, colocalization between them can be identified as “yellow” in an overlaid image. As such, colocalization studies can be subject to misinterpretation and inconsistencies [see, e.g., 1, 2]. To address this concern, numerous approaches have been proposed moving colocalization towards more rigorous and robust quantification [see, e.g., 3, 4, 5, 6, 7, among many others].

Arguably the most widely-used quantitative measures for colocalization are Pearson's correlation coefficient and Manders' split coefficients. Pearson's correlation coefficient was first introduced to the microscopy community by [3]. It measures the *linear relationship* of the intensities between the two channels, and a strong correlation indicates that a large intensity in one channel is often associated with a large intensity in the other. Another popular colocalization measure

is the Manders' split coefficients proposed by [4]. These coefficients measure fractions of signal in one channel that overlap with the other.

Pearson's correlation coefficient and Manders' split coefficients measure the degree of colocalization manifested in two distinct ways: correlation and co-occurrence, respectively. The former is most appropriate if two probes co-distribute proportionally to each other; whereas the latter is most useful if simple spatial overlap between the two probes is expected. We argue that both can be characterized as metrics of specific types of *positive dependence*. In statistical jargon, both Pearson's correlation coefficient and Manders' split coefficients are *parametric* in nature, which means that they work best when specific modeling assumptions hold; for example, Pearson's correlation works when the relationship between channels is linear. However, given the complexities that exist within biological contexts when measuring colocalization, this motivates us to consider a more robust method to quantify more general positive dependencies between two probes. To this end, we cast the colocalization analysis as a nonparametric statistical testing problem. The approach we introduce for the testing problem here is naturally *nonparametric*, which works under much more general circumstances, as colocalization may display other types of associations beyond correlation or co-occurrence and may not be captured effectively by these two classical methods. The idea of nonparametric correlation coefficient in colocalization analysis has previously been introduced, e.g. [8, 9]; however our work is the first to conduct colocalization analysis in a fashion of rigorous nonparametric statistical testing so that false discovery can be better controlled and the value of coefficients can be transformed into statistical significance for easier interpretation.

Not only is the biology itself adding complexity to colocalization analyses, but added complications are introduced during the acquisition process of biological samples, including varying background levels, leading to the need for extensive pre-processing before colocalization analyses can be applied. When applying either Pearson's correlation coefficient or Manders' split coefficients to dual-channel fluorescence microscopic images directly, one might ignore an important fact that a dark background with positive offset may occupy a substantial area of the image. The power of either method critically depends on one's ability to determine an appropriate background level. Oftentimes, the solution is to avoid or exclude background pixels through manual selection a region of interest [10, 7]. More principled approaches have also been

^{*}Columbia University

[†]University of Wisconsin-Madison

[‡]Morgridge Institute for Research

[§]Address for Correspondence: Department of Statistics, Columbia University, 1255 Amsterdam Avenue, New York, NY 10027.

considered. In particular, global threshold reduction [see, e.g., 5] and local median threshold reduction [see, e.g., 6, 10, 7] have been widely used. In general, determining the background is a complex process and very susceptible to misspecification, as well as a lack of reproducibility. There is a need for more robust colocalization analyses that can tease out the hidden, true biology without the need for user-based interference and manipulation via these pre-processing steps. The approach we developed here automatically adjusts for background, and therefore addresses this challenge in a seamless fashion.

In this paper, we discuss the main ideas behind different quantification techniques of colocalization and introduce our approach as a more general and robust alternative to those most frequently used. We provide a more rigorous justification of the proposed approach and show that the proposed colocalization score yields optimal test of colocalization under mild regularity conditions. Numerical experiments, both simulated and real, are also presented to further demonstrate the merits of our proposed method.

II. ROBUST QUANTIFICATION OF COLOCALIZATION

To emphasize the need for a more robust quantification of colocalization, we first note that the usefulness of either Pearson's correlation coefficient or Manders' split coefficients relies on certain parametric assumptions about the data, albeit implicitly. Let \mathbb{I} be the index set for all pixels in an image or a region of interest and, denoted by the pair (X_i, Y_i) , the intensity of the two channels measured at pixel $i \in \mathbb{I}$. Then the Pearson's correlation coefficient between two channels is given by

$$r = \frac{\sum_i (X_i - \bar{X})(Y_i - \bar{Y})}{\sqrt{\sum_i (X_i - \bar{X})^2 \sum_i (Y_i - \bar{Y})^2}}, \quad (1)$$

where \bar{X} and \bar{Y} are the average intensities of the two channels, respectively. As mentioned previously, Pearson's correlation only measures the linear relationship of the intensities between two channels, and therefore may not be able to capture colocalization to its full extent. Consider a simple example where intensities (X, Y) from the two channels can be modeled as a bivariate log-normal distribution. More concretely, $(\log(X), \log(Y))$ follows a bivariate normal distribution with mean 0, variance $3^2 = 9$, and correlation coefficient ρ so that the average intensity for each channel is approximately 90. The left panel of Figure 1 gives the (population) Pearson's correlation coefficient between X and Y as a function of ρ (i.e. the Pearson's correlation between $\log(X)$ and $\log(Y)$) and clearly shows that even very strong linear relationships on the log-scale may result in only modest Pearson correlation coefficients. In other words, Pearson's correlation is heavily influenced by nonlinear transformation on each channel. To further demonstrate this potential deficiency, 4×4 images in two channels are given in the two right panels of Figure 1, whose intensities were generated from lognormal distribution with $\rho = 0.9$. Despite the apparent colocalization between the two channels, both in terms of ρ and visually, the Pearson's correlation coefficient is a mere 56%.

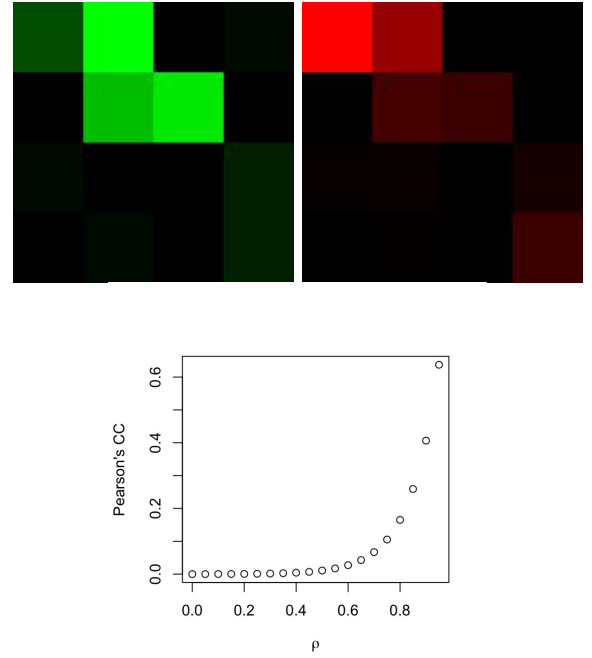


Fig. 1: Pearson's correlation coefficient is limited in that it only measures linear relationships between two channels. The lower panel shows the (population) correlation coefficient as a function of the correlation coefficient on the log-scale. The two upper panels show sample images which, on the log-scale, have a correlation coefficient of 90%; yet, on the original scale, it is only 56%.

There are similar deficiencies for Manders' split coefficients as well. Specifically, Manders' split coefficients are defined by

$$M_1 = \frac{\sum_{i:Y_i > \alpha_Y} X_i}{\sum_{i \in \mathbb{I}} X_i} \quad \text{and} \quad M_2 = \frac{\sum_{i:X_i > \alpha_X} Y_i}{\sum_{i \in \mathbb{I}} Y_i},$$

where the two thresholds α_X and α_Y are chosen appropriately so that any intensities below their respective threshold can be deemed as "background". It is worth noting that M_1 and M_2 can also be viewed as measures of the linear relationship between X_i s and $\mathbf{1}(Y_i > \alpha_Y)$ s, and Y_i s and $\mathbf{1}(X_i > \alpha_X)$ s, respectively, where $\mathbf{1}(\cdot)$ is the indicator function. In other words, despite their differences in appearance, both Pearson's correlation and Manders' split coefficients can be viewed as measures for linear relationships between X_i s and Y_i s or their specific *monotonic transformations*. Motivated by this observation, we can consider a more general metric for dependence between X_i s and Y_i s under *arbitrary* monotonic transformations; more specifically, we have opted to quantify colocalization by Kendall's tau.

Let $n = |\mathbb{I}|$, the cardinality of \mathbb{I} . We call a pair of observations (X_i, Y_i) and (X_j, Y_j) ($i \neq j$) concordant if $\text{sign}(X_i - X_j)\text{sign}(Y_i - Y_j) > 0$ and discordant if otherwise. Kendall tau for $\{(X_i, Y_i) : i \in \mathbb{I}\}$ is then defined as the difference between the number of concordant pairs and discordant pairs divided by the total number of pairs, that is,

$$\tau = \frac{1}{n(n-1)} \sum_{i \neq j} \text{sign}(X_i - X_j)\text{sign}(Y_i - Y_j).$$

It is clear that τ depends on the data $\{(X_i, Y_i) : i \in \mathbb{I}\}$ only through their ranks among X_i s and Y_i s so that it is invariant with respect to any monotonic transformations of X_i s and Y_i s.

As any other metric, when using τ to measure the degree of colocalization, it is essential to correct for background, and it may be fruitless to assess colocalization at locations where both channels are void of any real signal. To this end, it is of interest to evaluate Kendall tau only on the subset of pixels where both channels are sufficiently bright, leading to

$$\tau(t_X, t_Y) = \frac{\sum_{i,j \in \mathcal{K}(t_X, t_Y): i \neq j} \text{sign}(X_i - X_j) \text{sign}(Y_i - Y_j)}{n_{t_X, t_Y}(n_{t_X, t_Y} - 1)},$$

where

$$\mathcal{K}(t_X, t_Y) = \{i \in \mathbb{I} : X_i \geq t_X, Y_i \geq t_Y\}$$

and

$$n_{t_X, t_Y} = |\mathcal{K}(t_X, t_Y)|,$$

for two pre-specified t_X and t_Y . We shall also adopt the convention that $\tau(t_X, t_Y) = -\infty$ if $n_{t_X, t_Y} \leq 1$.

Obviously, in practice, we do not know at which level t_X and t_Y colocalization may occur. To overcome this problem, we consider instead the maximum of normalized Kendall tau correlation for all possible t_X s and t_Y s. Note that the variance of $\tau(t_X, t_Y)$, when X is independent from Y , is

$$2(2n_{t_X, t_Y} + 5)/9n_{t_X, t_Y}(n_{t_X, t_Y} - 1).$$

We shall therefore consider the following metric for colocalization

$$\tau^* := \max_{\substack{t_X \geq X_{(\lfloor n/2 \rfloor)}, \\ t_Y \geq Y_{(\lfloor n/2 \rfloor)}}} \left\{ \tau(t_X, t_Y) \cdot \sqrt{\frac{9n_{t_X, t_Y}(n_{t_X, t_Y} - 1)}{2(2n_{t_X, t_Y} + 5)}} \right\},$$

where $X_{(k)}$ and $Y_{(k)}$ are the k th order statistics of X_i s and Y_i s respectively. Note that the lower bounds $X_{(\lfloor n/2 \rfloor)}$ and $Y_{(\lfloor n/2 \rfloor)}$ are chosen for convenience and can be replaced by other values. In particular, they can be taken as approximated thresholds of signal so that only possible thresholds above those approximated are considered.

The nonparametric version colocalization measure τ^* is more robust in at least two ways, compared to Pearson's correlation coefficient or Manders' split coefficients. τ^* is invariant with respect to arbitrary monotonic transformations of X and Y . Furthermore, τ^* only takes real correlation on signal into account and is immune from the presence of background. To demonstrate the merit of τ^* , we discuss the theoretical properties of τ^* under appropriate models in the next section.

Remark: The non-parametric correlation coefficient can reflect the general associations between variables in a more precise way, compared with parametric correlation coefficient [see, e.g. 11, 12]. To illustrate this, we consider two examples to compare the Kendall tau correlation coefficient τ we use here and one of the most widely used correlation coefficient, Pearson correlation coefficient r . The first example is when X and Y are drawn from independent t -distributions with degrees of freedom less than 4. In this case, the variance of Pearson's correlation coefficient r is not well defined [see, e.g. 11], so

that r might deviate from 0 with large probability. On the other hand, Kendall tau correlation converges to 0 as the sample size increases, as long as X and Y are independent, immune from any heavy tail distributions. In the second example [see, e.g. 12], X is drawn from a log-normal distribution and $Y = X^S$ for some integer S . The Pearson's correlation coefficient between X and Y is

$$\frac{e^S - 1}{\sqrt{(e - 1)(e^{S^2} - 1)}} \rightarrow 0, \quad \text{as } S \rightarrow \infty,$$

despite the fact that Y is totally determined by X . However, the Kendall tau correlation between X and Y is always 1, reflecting the strong connection between X and Y . This suggests Kendall tau correlation τ is able to capture a wider range of association than Pearson's correlation coefficient r . Therefore, Kendall's tau τ can reflect correlation more precisely than Pearson's correlation coefficient r .

III. STATISTICAL SIGNIFICANCE

To translate the proposed metric for colocalization τ^* into statistical significance, we now consider a hypothesis testing framework for colocalization. To this end, F denotes the joint distribution function for the pair (X_i, Y_i) , where $i = 1, \dots, n$. In the absence of colocalization (null hypothesis, H_0), the two channels can be expected to behave independently so that

$$H_0 : F(x, y) = F_X(x)F_Y(y), \quad \forall x, y \in \mathbb{R}, \quad (2)$$

where $F_X(x) = F(x, +\infty)$ and $F_Y(y) = F(+\infty, y)$ are the marginal distribution functions. On the other hand, in the presence of colocalization (alternative hypothesis, H_1), we expect that X and Y are positively dependent. Furthermore, positive dependency only applies to signals; that is, there exists some η_X and η_Y such that the conditional distribution of (X, Y) given that $X > \eta_X$ and $Y > \eta_Y$, hereafter denoted by F_{η_X, η_Y} , is *positively quadrant dependent*. Specifically, if F_{η_X, η_Y} is positively quadrant dependent, then $F_{\eta_X, \eta_Y}(x, y) \geq F_{\eta_X}(x)F_{\eta_Y}(y)$ for all $x, y \in \mathbb{R}$, and there exist $x, y \in \mathbb{R}$ such that $F_{\eta_X, \eta_Y}(x, y) > F_{\eta_X}(x)F_{\eta_Y}(y)$ where $F_{\eta_X}(x) = F_{\eta_X, \eta_Y}(x, +\infty)$ and $F_{\eta_Y}(y) = F_{\eta_X, \eta_Y}(+\infty, y)$ are the marginal distributions of F_{η_X, η_Y} [see, e.g., 13, 14]. We do not assume prior knowledge of η_X and η_Y so that

$$H_1 : \exists \eta_X, \eta_Y \text{ s.t. } F_{\eta_X, \eta_Y} \text{ is positively quadrant dependent.}$$

The colocalization metric τ^* can be used to effectively test H_0 against H_1 and therefore can be converted into p-values as a scale-free measure of colocalization, which we will discuss in more detail in the next section.

A. Optimality

As previously stated, the colocalization metric τ^* provides an efficient statistic for testing H_0 against H_1 . To this end, let q_α denote the $1 - \alpha$ quantile of the distribution of τ^* under H_0 . Although there is no closed-form analytic expression for τ^* , it can be readily evaluated by Monte Carlo schemes. We shall discuss in further details practical issues of implementation in the next subsection. Once q_α is computed, we can then proceed to reject H_0 and therefore claim colocalization as soon

as the observed τ^* is greater than q_α . We denote this test by Δ . It is clear that Δ is an α level test; we now argue that it is also optimal in the sense that it can detect evidence of colocalization at a level that no other tests could improve.

Note first that positive quadrant dependence of F_{η_X, η_Y} immediately implies that for two independent copies (X, Y) and (\tilde{X}, \tilde{Y}) following distribution F ,

$$\begin{aligned} T(\eta_X, \eta_Y) &:= \\ \mathbb{P} \left\{ (X - \tilde{X})(Y - \tilde{Y}) > 0 \mid X, \tilde{X} > \eta_X; Y, \tilde{Y} > \eta_Y \right\} - \\ \mathbb{P} \left\{ (X - \tilde{X})(Y - \tilde{Y}) < 0 \mid X, \tilde{X} > \eta_X; Y, \tilde{Y} > \eta_Y \right\} &> 0. \end{aligned}$$

In other words, under null hypothesis H_0 , $T(\eta_X, \eta_Y) = 0$, for all η_X, η_Y ; while under the alternative hypothesis H_1 ,

$$\sup_{\eta_X, \eta_Y} T(\eta_X, \eta_Y) > 0.$$

Theorem 1. Assume that $\{(X_i, Y_i) : i \in \mathbb{I}\}$ ($n := |\mathbb{I}|$) are independently sampled from F obeying

$$\sup_{\eta_X, \eta_Y} V(\eta_X, \eta_Y) \cdot T^2(\eta_X, \eta_Y) \gg \frac{\log \log n}{n}. \quad (3)$$

Here $V(\eta_X, \eta_Y) := 1 + F(\eta_X, \eta_Y) - F_X(\eta_X) - F_Y(\eta_Y)$. Then Δ is a consistent test in that we reject H_0 in favor of H_1 with probability tending to one. Conversely, there exists a constant $c > 0$ such that for any α -level test Δ based on sample $\{(X_i, Y_i) : i \in \mathbb{I}\}$, there is an instance where joint distribution function F obeying

$$\sup_{\eta_X, \eta_Y} V(\eta_X, \eta_Y) \cdot T^2(\eta_X, \eta_Y) \geq c \frac{\log \log n}{n} \quad (4)$$

and yet, we accept H_0 with probability tending to $1 - \alpha$ as if H_0 holds.

Hereafter, we write $a_n \gg b_n$ if $b_n = o(a_n)$. Theorem 1 provides theoretical justifications that τ^* is an appropriate and powerful test statistic for H_0 against H_1 . In particular, it suggests that τ^* is optimal in the sense that it can detect correlation at a level no other tests could significantly improve.

B. Practical Considerations

In practice, it is more useful to report the p-value associated with an observed τ^* rather than just a simple decision on rejecting or accepting the null hypothesis H_0 . To this end, we can compare the observed τ^* from a dual-channel microscopic image with the sampling distribution of τ^* when there is no colocalization. We can apply a permutation test to estimate the sampling distribution of τ^* under H_0 . More specifically, we can randomly shuffle $\{X_i : i \in \mathbb{I}\}$ or $\{Y_i : i \in \mathbb{I}\}$. Random arrangement ensures that there is no meaningful colocalization between the two channels. For each shuffled or permuted sample, we recompute τ^* . The null distribution of τ^* can therefore be estimated by repeating the random rearrangement many times.

When implementing this strategy, there are two practical challenges. The first potential hurdle is the computational cost. It is not hard to see that

$$\tau^* = \max_{\substack{t_X = X_{(j)}, \\ t_Y = Y_{(k)}: \\ j, k \geq \lfloor n/2 \rfloor}} \left\{ \tau(t_X, t_Y) \cdot \sqrt{\frac{9n_{t_X, t_Y}(n_{t_X, t_Y} - 1)}{2(2n_{t_X, t_Y} + 5)}} \right\}. \quad (5)$$

There are a total of $O(n^2)$ possible pairs of (j, k) , and fast evaluation of Kendall tau requires $O(n \log n)$ floating-point operations. Thus, the exact computation of τ^* has complexity $O(n^3 \log n)$. This could be quite expensive to compute for even a moderately-sized image, and particularly so because we need to compute τ^* for many scrambled images.

To this end, we propose to compute an approximation of τ^* . More specifically, instead of evaluating the maximum over $O(n^2)$ possible pairs of (j, k) as in (5), we consider the maximum over only a subset of these pairs. Let

$$\mathcal{R}_n := \left\{ s : s = \left\lfloor n - \left(1 + \frac{1}{\log \log n}\right)^j \right\rfloor, j \in \mathbb{N}_+, s \geq \lfloor n/2 \rfloor \right\}.$$

Here \mathbb{N}_+ refers to the set of all positive integers. In other words, \mathcal{R}_n is a collection of coordinates that are nearly a geometric series. As such, the number of pairs in \mathcal{R}_n is much smaller than the original ones, as illustrated in Figure 2.

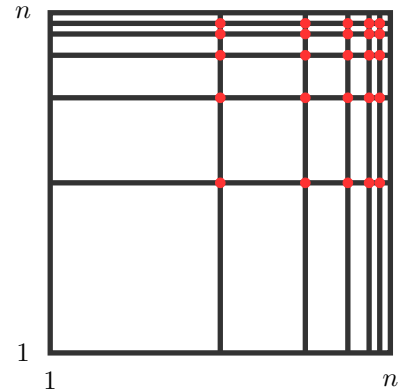


Fig. 2: All possible pairs (j, k) when both j and k are in \mathcal{R}_n

We then define

$$\tau_{\text{app}}^* := \max_{\substack{t_X = X_{(j)}, \\ t_Y = Y_{(k)}: \\ j, k \in \mathcal{R}_n}} \left\{ \tau(t_X, t_Y) \cdot \sqrt{\frac{9n_{t_X, t_Y}(n_{t_X, t_Y} - 1)}{2(2n_{t_X, t_Y} + 5)}} \right\}. \quad (6)$$

A careful inspection of the proof of Theorem 1 shows that a test that uses τ_{app}^* in place of τ^* remains optimal and consistent under condition (3). The idea of evaluating a statistic on an approximation set only to reduce the computation cost while retaining statistical power is commonly used in scan statistics [see, e.g., 15, 16, 17, 18, 19]. The fast τ_{app}^* can be applied to large scale microscopic images, as its computational complexity is almost linear with the number of pixels.

Another practical challenge is the potential dependence among X_i s and Y_i s. The range of dependence within either channel is often determined by the numerical aperture of the

objective lens, and the fluorescence emission wavelength, as shown previously by [5]. It is important that we preserve such a dependence structure when estimating the sampling distribution of τ^* . To this end, we can adopt the strategy advocated by [5]; instead of scrambling the image pixel-by-pixel, we can divide the image into blocks with the number of pixels in each block determined by the point spread function and then scramble the image block-by-block.

With these two adjustments, we are ready to show the whole flow of our new method. In Algorithm 1, the input image can be an image before or after pre-processing. According to our experience, our method works very well on both raw images (see Section IV-C) and pre-processed images (see Section IV-B). It is also worth noting that the p -value obtained in Algorithm 1 is only calculated for a single experiment. Multiple comparison correction is needed if we apply Algorithm 1 on multiple images. Algorithm 1 has been implemented in R package `RKColocal`, which is openly available (see <https://github.com/lakerws/RKColocal>).

Algorithm 1 our new method based on τ^* (or τ_{app}^*)

Input: channel intensities $\{X_i\}_{i \in \mathbb{I}}$, $\{Y_i\}_{i \in \mathbb{I}}$, repeating times B and block size D

Output: p -value

$E_0 \leftarrow$ calculate τ^* (or τ_{app}^*) on $\{X_i\}_{i \in \mathbb{I}}$ and $\{Y_i\}_{i \in \mathbb{I}}$.

for $j = 1$ to B **do**

$\{\tilde{X}_i\}_{i \in \mathbb{I}} \leftarrow$ block-wise randomly shuffle $\{X_i\}_{i \in \mathbb{I}}$ with block size D

$E_j \leftarrow$ calculate τ^* (or τ_{app}^*) on $\{\tilde{X}_i\}_{i \in \mathbb{I}}$ and $\{Y_i\}_{i \in \mathbb{I}}$

end for

$P \leftarrow \#\{E_j > E_0\}/B$

return P

IV. NUMERICAL EXPERIMENTS

To demonstrate the merits of our proposed method, we conducted several sets of numerical experiments, applying our method on both simulated and biological image data.

A. Simulated Data Examples

To simulate the positive dependence between the two channels, we consider a setting based on Clayton copula [see, e.g., 14]. More specifically, under the null hypothesis H_0 (no colocalization), we simulated the intensities of each pixel X and Y according to

$$X = e^{8(U-0.5)} \quad \text{and} \quad Y = e^{8(V-0.5)}, \quad (7)$$

where U and V are independently drawn from a uniform distribution between 0 and 1, $Unif([0, 1])$. The image is blurred by applying gaussian smoothing (point-spread function (PSF) is gaussian kernel) after intensities of each pixel are simulated following the rule above. A typical example of a simulated dual channel image without colocalization is shown in the left most column of Figure 3. To generate colocalization under the

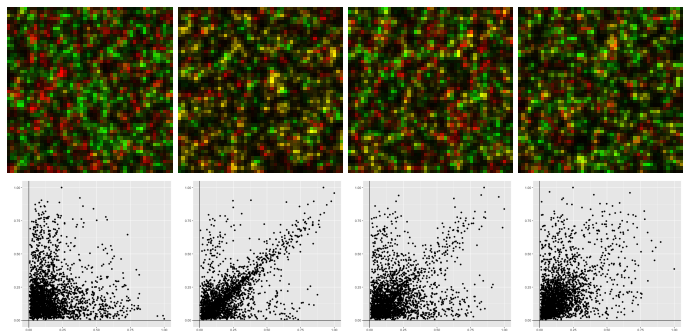


Fig. 3: Example images of simulated dual-channel data and their corresponding scatter plots (image size: 50×50). From left to right: an example simulated dual-channel image without colocalization (under the null hypothesis H_0), with colocalization when $R = 0.3$ and $\theta = 100$ (under the alternative hypothesis H_1), with colocalization when $R = 0.5$ and $\theta = 100$ (under the alternative hypothesis H_1), and with colocalization when $R = 0.3$ and $\theta = 5$ (under the alternative hypothesis H_1).

alternative hypothesis H_1 , we first simulated bivariate random variables (U, V) from a distribution:

$$\frac{d^2 F(u, v)}{dudv} = \begin{cases} g_\theta \left(\frac{u-R}{1-R}, \frac{v-R}{1-R} \right) & (u, v) \in [R, 1] \times [R, 1] \\ 1 & (u, v) \in [0, 1]^2 \setminus [R, 1]^2 \end{cases}$$

where $g_\theta(u, v)$, $0 < \theta < \infty$, is the density function of Clayton copula distribution, that is

$$g_\theta(u, v) = \frac{d^2}{dudv} (u^{-\theta} + v^{-\theta} - 1)^{-1/\theta} \\ = (\theta + 1)(uv)^{-(\theta+1)} (u^{-\theta} + v^{-\theta} - 1)^{-(2\theta+1)/\theta}.$$

Here, R is a parameter between 0 and 1, representing a threshold above which colocalization occurs, as positive quadrature dependence occurs when $U, V > R$. A larger R suggests colocalization occurs with less signal, so that detection of the colocalization is more difficult (compared to the second and third column in Figure 3). Another parameter, θ , is a number larger than 0, controlling the the dependence/colocalization level above the thresholds R . Specifically, the degree of positive quadrature dependence when $U, V > R$ is $\theta/(\theta + 2)$ i.e. $T(R, R) = \theta/(\theta + 2)$. Thus, a larger θ implies higher correlation among the given signal (compared to the second and fourth column in Figure 3). The pixel intensities (X, Y) follow the same monotone transformation of (U, V) in (7), and the image is also blurred by gaussian smoothing. The three right images of Figure 3 show examples of dual channel images with varying colocalization.

In this simulation experiment, we compared our new method with the traditional colocalization quantitative measures, including Pearson's correlation coefficient r and Manders' split coefficients M_1, M_2 . In M_1 and M_2 , the thresholds α_X and α_Y were chosen by applying Otsu's method to each channel. To make a comparison possible, we employed a statistical hypothesis testing framework and reported the decision associated with each quantitative measure. Specifically, we simulated

the null distribution¹ of colocalization quantitative measures, r , M_1 , M_2 or τ_{app}^* , and identified the upper 5% quantile of the null distribution as the critical value based on 1000 Monte Carlo simulations. In this way, we can ensure that the Type I error (the probability of false discovery) is controlled at level 5% up to Monte Carlo simulation error. The reported decision rejects the null hypothesis if the corresponding colocalization quantitative measure exceeded its respective critical value, failing to reject the null hypothesis otherwise. Under this statistical hypothesis testing framework, the performance of colocalization quantitative measures can be assessed through the power of testing, i.e. the probability of rejecting the null hypothesis under the alternative hypothesis H_1 . In this simulation study, the power β is estimated by the proportion of null hypothesis rejection, i.e.

$$\beta = \frac{\text{number of null hypothesis rejection}}{\text{number of simulation runs}}. \quad (8)$$

Clearly, a larger power β suggests the colocalization measure is more efficient in colocalization detection.

To investigate the performance of different colocalization measures, we compare their power β defined in (8) when data is generated according to the alternative hypothesis model (colocalization exists) under different values of R and θ . We conducted the simulation experiments by varying parameters R and θ in the alternative hypothesis model simultaneously. Specifically, we considered different values of R : 0.7, 0.8, and 0.9 and a range of θ from 1 to 10. For each combination of R and θ , we repeated the experiment 1000 times. In each experimental run, we simulated colocalized data on a 50×50 lattice and applied tests of r , M_1 , M_2 , or τ_{app}^* on the simulated data. The decision of each colocalization measure was recorded and the power β in 1000 experiments was calculated by (8). The results of power β are summarized in Figure 4. In Figure 4, the power β of all methods increases along with θ increasing and R decreasing, which is consistent with our discussion in the simulation setting introduction. These results show that the power β of our new method is larger than that of Pearson's correlation coefficient and Manders' split coefficients at most R and θ , especially when there is less colocalized signal (i.e. R is large). Therefore, we can conclude that τ_{app}^* out-performs r , M_1 , and M_2 .

B. Benchmark Real Data Examples

Next, we applied our new method to several benchmark real data examples from [6]. The first example detected colocalization between the ryanodine receptor (RyR) and the estrogen receptor alpha (ER α) in a mouse heart cell (in Figure 5a). As described in [6], there is no evidence that these two proteins interact. The second example compared the distribution of RyR and α 1C calcium channel (α 1C) in a mouse cell, which are known to colocalize (in Figure 5b). The third example measured the behavior of the α -subunit of Ca²⁺ and voltage-dependent large conductance K channels (MaxiK- α) and that of α -tubulin (in Figure 5c). These two types of proteins are partially colocalized according to [6].

¹Null distribution is the distribution of the test statistic, i.e. r , M_1 , M_2 , or τ_{app}^* , under the null hypothesis H_0 .

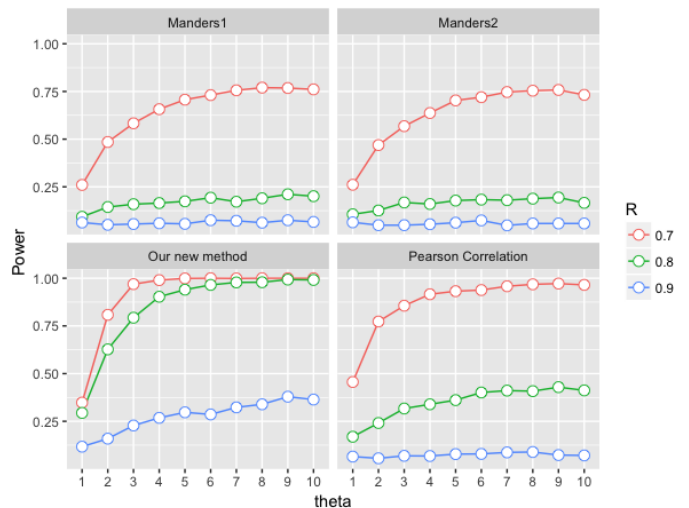


Fig. 4: The power comparison among colocalization quantitative measures under Clayton copula model. In each plot, the x axis is the value of θ and y axis is the value of power β (between 0 and 1). Different colors of curve represent different values of R .

For each of the three examples, the proposed metric τ_{app}^* and the histogram of its null distributions obtained via block-wise permutations are given in Figure 5. In these experiments, the number of permutations is 1000 and block size is $\lfloor \min(\sqrt{a}, \sqrt{b}) \rfloor$ when the size of image is $a \times b$. These results are fairly consistent with those reported in [6]. It is worth noting that [6] also ran many existing methods, including Pearson correlation coefficient and Manders' split coefficients, on these data examples and concluded that such quantification methods are prone to false discovery. In particular, both Pearson correlation coefficient and Manders' split coefficients identified colocalization in the first example [see 6], contrary to the biology behind it (in Figure 5a).

C. Real Data Examples

Finally, we applied our new method to real biological datasets. The first example is a set of microscopic images (image size: 1024×1024) of HeLa cells expressing the structural protein, Gag, of human immunodeficiency virus type 1 (HIV-1). HIV-1 virus particles assemble at the plasma membrane and are composed of ~ 2000 molecules of Gag [20, 21]. We applied the same analysis procedures as for the previous sections. There are three conditions with corresponding images. In the first two conditions (Figure 6a and Figure 6b), HIV-1-Gag (green channel) was fused to cyan fluorescence protein (CFP) and MS2 protein (red channel) was fused to yellow fluorescent protein (YFP). When expressed in cells as the only viral factor, HIV-1-Gag primarily forms particles at the edge of cells; these particles are only occasionally internalized by the cell and then observed near the nucleus. In the first condition, MS2 protein was designed to remain in the nucleus (Figure 6a), resulting in a negative control with low levels of colocalization between Gag-CFP and MS2-YFP. In the second

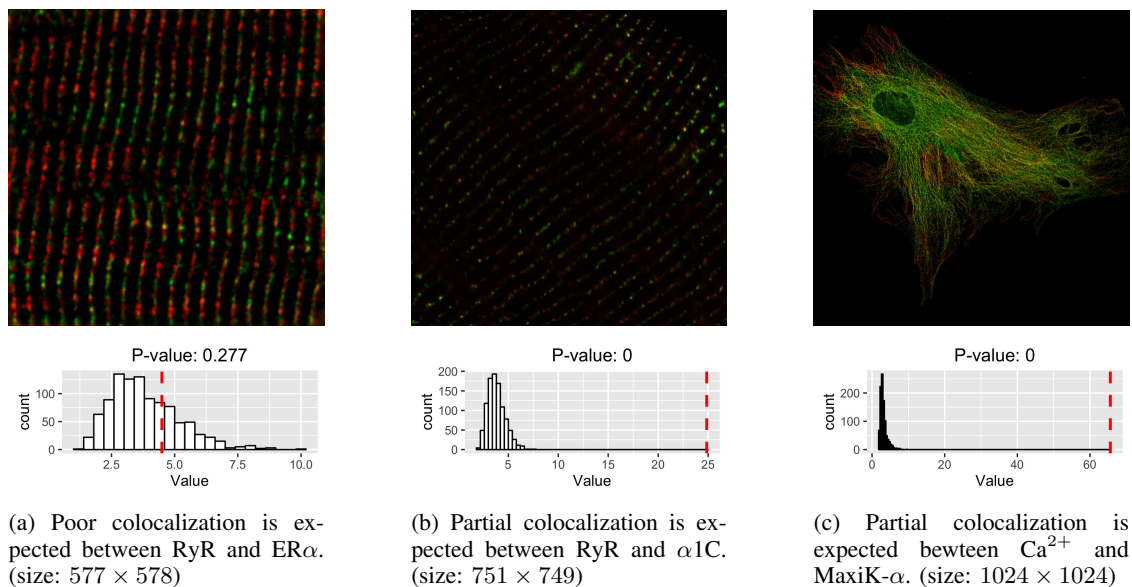


Fig. 5: Colocalization analysis result of τ_{app}^* on benchmark real data examples from [6].

condition (Figure 6b), Gag-CFP was expressed from an mRNA engineered to contain multiple copies of an RNA stem loop that binds MS2-YFP with high specificity [22]. Therefore, we expected significantly higher colocalization levels between Gag-CFP and MS2-YFP in Figure 6b as compared to those in Figure 6a. We summarized p -values and the corresponding approximated null distributions in Figure 6. The results show colocalization was discovered in Figure 6b if we rejected the null hypothesis when the p -value was smaller than 10%. On the other hand, no significant colocalization was found as p -values in Figure 6a were both larger than 70%. In the final condition (Figure 6c), two constructs expressing synthetic Gags were fused to CFP and YFP, respectively. As Gag should self-assemble into multi-colored particles, we expected the highest levels of colocalization in this condition between Gag-CFP and Gag-YFP as compared to the two previous conditions. After applying our new method on these images, we obtained a very strong, significant level of colocalization, with p -values far less than 0.1%.

We also applied our new method to another set of biological datasets. These microscopic images (image size: 512 \times 512) represent snapshots of a model used to elucidate signal responses during cellular wounding and the subsequent repair process. Rho GTPases, including Rho and Cdc42, control an enormous variety of processes and play a role during *Xenopus* oocyte wound repair [23]; however, they do not overlap during the wound repair process and therefore resulted in low levels, p -values larger than 85%, of detectable colocalization (Figure 7a). Calcium is an initially crude signal in wound repair, and PKC β participates in Rho and Cdc42 activation and is also recruited to cell wounds [24]. Calcium defines a broad region within which PKC β can be found, and therefore, some level of colocalization is expected, which was easily detected using our method (Figure 7b). Finally, Rho GTPases including Rho and Cdc42, have also been implicated in cortical cytoskeleton repair, so the actin regulatory protein, cortactin,

largely overlaps with Cdc42, for example, during the wound healing process. The highest levels of colocalization were expected between Cdc42 and cortactin within this group of images, and this was measured by our method (Figure 7c). Once again, this work demonstrates our new method's robustness within complex, biological contexts.

For the microscopic images of both biological datasets, we also applied Pearson correlation coefficient r and Manders' split coefficients (M_1, M_2). For M_1 and M_2 , the thresholds α_X and α_Y are still determined by Otsu's method. In τ_{app}^* , the lower bound of thresholds scanned was chosen as maximum of Otsu's threshold and median value. To obtain a p -value, the microscopic images were permuted block-wise as described in Section III-B. In these experiments, 1000 permutations were carried out and the block size was 32, the square root of the size of the image. The value of colocalization measures and corresponding p -values calculated by the permutation test are summarized in Table I. The results in Table I suggest that our new statistics τ_{app}^* is able to control false discovery far better than Pearson correlation coefficient and Manders' split coefficients. Moreover, the value of our τ_{app}^* and corresponding p -value can reflect the level of colocalization more precisely. It is worth noting that the size of the newly proposed index τ_{app}^* can also be affected by the area of colocalized region. In other words, τ_{app}^* is relatively small when the colocalization happens in a small region. For example, τ_{app}^* is relatively small (p -value is relatively large) in Figure 6b when colocalization only concentrates at the edge of cell.

V. CONCLUDING REMARKS

In this paper, we propose a new robust measure of colocalization. Due to the intrinsic, nonparametric characteristic of Kendall's tau correlation coefficient, the new colocalization measure captures a wider range of associations between two channels than most existing parametric quantitative measures, such as Pearson's correlation coefficient and Manders' split

| | | Pearson r | | Manders M_1 | | Manders M_2 | | New measure τ_{app}^* | |
|-----------------------------------|-------|-------------|------------|---------------|------------|---------------|------------|-----------------------------------|------------|
| | | r | p -value | M_1 | p -value | M_2 | p -value | τ_{app}^* | p -value |
| Figure 6a (Poor colocalization) | left | 0.599 | < 0.1% | 0.425 | < 0.1% | 0.122 | < 0.1% | 6.328 | 86.6% |
| | right | 0.581 | < 0.1% | 0.276 | < 0.1% | 0.102 | < 0.1% | 4.922 | 70.2% |
| Figure 6b (Good colocalization) | left | 0.843 | < 0.1% | 0.629 | < 0.1% | 0.308 | < 0.1% | 42.659 | 9.2% |
| | right | 0.909 | < 0.1% | 0.629 | < 0.1% | 0.355 | < 0.1% | 115.191 | < 0.1% |
| Figure 6c (Strong colocalization) | left | 0.972 | < 0.1% | 0.552 | < 0.1% | 0.658 | < 0.1% | 501.111 | < 0.1% |
| | right | 0.983 | < 0.1% | 0.609 | < 0.1% | 0.539 | < 0.1% | 489.459 | < 0.1% |
| Figure 7a (Poor colocalization) | | 0.486 | < 0.1% | 0.206 | < 0.1% | 0.123 | < 0.1% | 1.691 | 85.1% |
| Figure 7b (Good colocalization) | | 0.850 | < 0.1% | 0.285 | < 0.1% | 0.178 | < 0.1% | 39.175 | < 0.1% |
| Figure 7c (Good colocalization) | | 0.291 | < 0.1% | 0.122 | < 0.1% | 0.104 | < 0.1% | 15.798 | < 0.1% |

TABLE I: The colocalization measure values and corresponding p -value obtained by Pearson’s correlation coefficient r , Manders’ split coefficients M_1 , M_2 and our new method τ_{app}^* on microscopic images in Figure 6 and Figure 7.

coefficients. Given the vast complexities in bioimage data and variable associations between two biological probes beyond simple linear correlation or co-occurrence, our new nonparametric measure provides a more accurate reflection on the given association. Scanning at different signal levels allows our new measure to discover potential associations between two probes automatically without knowledge of thresholds for background. Under statistical hypothesis testing framework, if we assume mild regular conditions for intensity distributions, the test based on our new colocalization score is able to achieve statistical optimality.

We also developed a user-friendly, fast algorithm for our new colocalization measure so that the colocalization score can be translated into statistical significance efficiently. To overcome the computational hurdle of scanning, we proposed an approximation of our new colocalization measure to accelerate computation. In doing so, the approximated colocalization score can be calculated much more efficiently. Furthermore, we adopted a block-wise permutation test as in [5] to evaluate the calculated p -value. Putting this all into a single algorithm, users are able to get a p -value with a single ‘click’. Results from several experiments using benchmark and biological data converge to the conclusion that our new algorithm remains highly efficient.

The algorithm is readily available in an R package, RKColocal, as described previously. This code is also currently being adapted for incorporation into ImageJ, a popular open-source bioimage analysis software package [see, e.g., 25]. This tool and its continued development will also help bridge statistics and bioimaging by providing such improved algorithms and methods that facilitate productive collaborations between fields.

Interdisciplinary, collaborative research can lead to more innovations and discoveries. When colocalization analyses are cast as statistical hypothesis testing problems, as shown in Section III, we tackled a bioimage processing problem with statistical techniques without losing perspectives from both communities. The statistical hypothesis testing framework not only helped us develop an efficient approach to detect interesting associations between probes, but also made sure that true associations between channels were always reported and false

discoveries kept under control. Through a statistical lens, our new nonparametric statistical approach is ultimately trustworthy and precise. We believe the same application of statistics can also be extended to other bioimage processing techniques, including deconvolution, spectral unmixing, lifetime analyses, and more. We anticipate more collaborative benefits at the intersection of bioimage processing and statistics in the future.

ACKNOWLEDGMENT

The authors would like to thank Nathan Sherer and Jordan Becker for sharing the microscopy image data sets in Figure 6, and William Bement for sharing the the microscopy image data sets in Figure 7.

APPENDIX PROOF OF THEOREM 1

The proof is somewhat lengthy, and we break it into several steps.

a) *Size of q_α* : We first show that

$$q_\alpha = O_p(\sqrt{\log \log n}).$$

Recall that q_α is the upper α quantile of τ^* under H_0 . It then suffices to show that there exists some universal constant C such that

$$\mathbb{P}\left(\tau^* \geq C\sqrt{\log \log n}\right) \rightarrow 0. \quad (9)$$

Observe that τ^* does not depend on the marginal distribution under H_0 , we can assume without loss of generality that $F(x, y) = 1_{(0 \leq x \leq 1, 0 \leq y \leq 1)}$. Let $G_n^X(t)$, $G_n^Y(t)$, and $G_n(t)$ be the empirical distribution functions of X , Y , and (X, Y) , respectively, that is

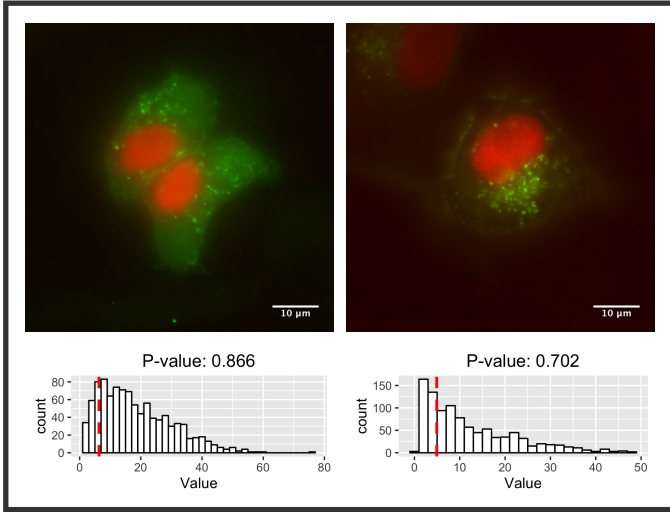
$$G_n^X(t) = \frac{1}{n} \sum_{i=1}^n I_{(X_i \geq t)}, \quad G_n^Y(t) = \frac{1}{n} \sum_{i=1}^n I_{(Y_i \geq t)},$$

and

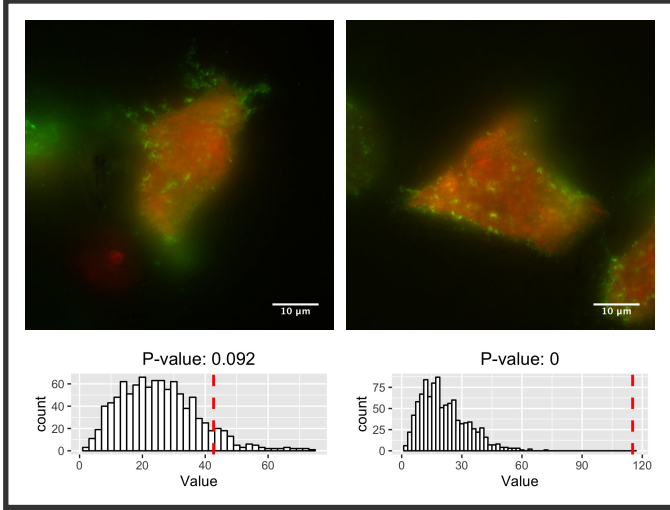
$$G_n(t, s) = \frac{1}{n} \sum_{i=1}^n I_{(X_i \geq t, Y_i \geq s)}.$$

Write

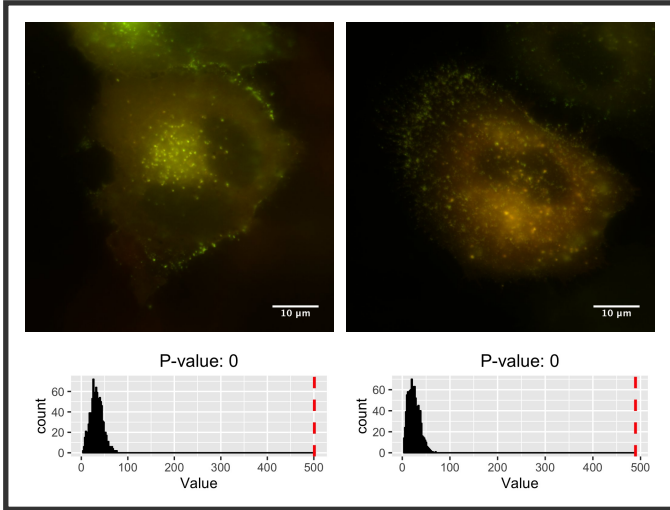
$$A_\alpha^X := \left\{ \sup_{1/2 \leq t < 1} \frac{|nG_n^X(t) - n(1-t)|}{\sqrt{n(1-t)}} \leq \alpha \sqrt{\log \log n} \right\},$$



(a) Poor colocalization examples (image size: 1024×1024): Low levels of colocalization between MS2-YFP and Gag-CFP are expected.



(b) Good colocalization examples (image size: 1024×1024): High level of colocalization between Gag-CFP and MS2-YFP are expected.



(c) Strong colocalization examples (image size: 1024×1024): The highest level of colocalization between Gag-CFP and Gag-YFP are expected.

Fig. 6: p -value and null distribution obtained by our new method on real data examples of Hella cells.

$$A_{\alpha}^Y := \left\{ \sup_{1/2 \leq t < 1} \frac{|nG_n^Y(t) - n(1-t)|}{\sqrt{n(1-t)}} \leq \alpha \sqrt{\log \log n} \right\},$$

and

$$A_{\alpha} := \left\{ \sup_{\substack{\log \log n/n \leq \\ L(t,s) \leq 1/2}} \frac{|nG_n(t,s) - nL(t,s)|}{\sqrt{nL(t,s)}} \leq \alpha \sqrt{\log \log n} \right\}.$$

Hereafter, we refer $L(t,s) = (1-t)(1-s)$. It is well known that there exists $\alpha_0 > 2$ such that

$$\mathbb{P}(A_{\alpha_0}^X \cap A_{\alpha_0}^Y \cap A_{\alpha_0}) \rightarrow 1, \quad n \rightarrow \infty.$$

See, e.g., [26]. Hence, it is sufficient to get (9) conditioned on $A_{\alpha_0}^X \cap A_{\alpha_0}^Y \cap A_{\alpha_0}$.

Recall that

$$\tau^* = \max_{j,k \geq \lfloor n/2 \rfloor} \tilde{\tau}(X_{(j)}, Y_{(k)}),$$

where

$$\tilde{\tau}(t_X, t_Y) = \tau(t_X, t_Y) \cdot \sqrt{\frac{9n_{t_X, t_Y}(n_{t_X, t_Y} - 1)}{2(2n_{t_X, t_Y} + 5)}}. \quad (10)$$

Write

$$\mathcal{I}_1 = \left\{ (j, k) \in [n]^2 : j, k \geq \lfloor n/2 \rfloor, nL\left(\frac{j}{n}, \frac{k}{n}\right) \leq \alpha_0^2 \log \log n \right\},$$

$$\mathcal{I}_2 = \left\{ (j, k) \in [n]^2 : j, k \geq \lfloor n/2 \rfloor, nL\left(\frac{j}{n}, \frac{k}{n}\right) > \log^2 n \right\},$$

and

$$\mathcal{I}_3 = \{(j, k) \in [n]^2 : j, k \geq \lfloor n/2 \rfloor, \alpha_0^2 \log \log n \leq nL\left(\frac{j}{n}, \frac{k}{n}\right) \leq \log^2 n\}. \quad (11)$$

It is clear that $\tau^* = \max\{\tau_1^*, \tau_2^*, \tau_3^*\}$ where

$$\tau_j^* = \max_{(j,k) \in \mathcal{I}_j} \tilde{\tau}(X_{(j)}, Y_{(k)}).$$

It therefore suffices to upper bound τ_j^* separately.

We begin with τ_1^* . Under the event $A_{\alpha_0}^X \cap A_{\alpha_0}^Y \cap A_{\alpha_0}$, we have

$$(1 - X_{(j)})(1 - Y_{(k)}) \leq \frac{2\alpha_0^2 \log \log n}{n},$$

when $n(1 - j/n)(1 - k/n) \leq \alpha_0^2 \log \log n$. As shown by [26],

$$\begin{aligned} & \mathbb{P}\left(\sup_{L(t,s) \leq 2\alpha_0^2 \log \log n/n} nG_n(t,s) \geq m\right) \\ & \leq c_1 \frac{(2c_2\alpha_0^2 \log \log n)^m}{m!} \log n. \end{aligned}$$

Hereafter, we shall use c to denote a generic positive constant that may take different values at each appearance. Taking $m = 2c_2\alpha_0^2 e^2 \log \log n$, we can ensure

$$\mathbb{P}\left(\sup_{L(t,s) \leq 2\alpha_0^2 \log \log n/n} nG_n(t,s) \geq 2c_2\alpha_0^2 e^2 \log \log n\right) \rightarrow 0.$$

This suggests

$$\mathbb{P}\left(\max_{(j,k) \in \mathcal{I}_1} n_{X_{(j)}, Y_{(k)}} \geq 2c_2\alpha_0^2 e^2 \log \log n\right) \rightarrow 0.$$

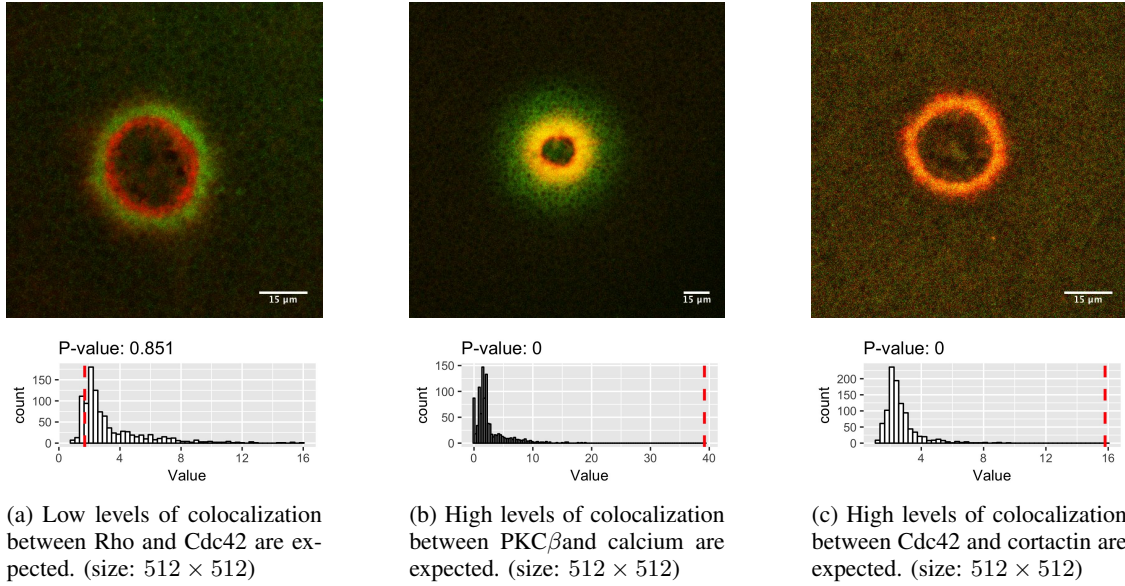


Fig. 7: p -value and null distribution obtained by our new method on real data examples of wound cell.

By definition of $\tilde{\tau}(t_X, t_Y)$,

$$\tilde{\tau}(t_X, t_Y) \leq \sqrt{\frac{9n_{t_X, t_Y}(n_{t_X, t_Y} - 1)}{2(2n_{t_X, t_Y} + 5)}}.$$

This immediately suggests

$$\mathbb{P}\left(\tau_1^* > \frac{3}{2}\sqrt{2c_2\alpha_0^2 e^2 \log \log n}\right) \rightarrow 0.$$

Next, we consider τ_2^* . Let

$$\mathcal{N}_n = \left\{ (j, k) : j, k \in \mathcal{S}_n \text{ and } nL\left(\frac{j}{n}, \frac{k}{n}\right) > \log^2 n \right\}$$

where \mathcal{S}_n is

$$\left\{ s : s = \left\lfloor n - \left(1 + \frac{\sqrt{\log \log n}}{\log n}\right)^j \right\rfloor, j \in \mathbb{N}_+, s \geq \lfloor n/2 \rfloor \right\},$$

and

$$\tau_{\mathcal{N}_n}^* := \max_{(j, k) \in \mathcal{N}_n} \tilde{\tau}(X_{(j)}, Y_{(k)}).$$

Our strategy is to first show the difference between $\tau_{\mathcal{N}_n}^*$ and τ_2^* is negligible and then bound $\tau_{\mathcal{N}_n}^*$.

To bound $\tau_2^* - \tau_{\mathcal{N}_n}^*$, we consider the following projection $\pi : \mathbb{N} \rightarrow \mathbb{N}$, which maps integer i to the largest integer in \mathcal{S}_n that is smaller than i . Conditioned on $A_{\alpha_0}^X \cap A_{\alpha_0}^Y \cap A_{\alpha_0}$,

$$\begin{aligned} & n_{X_{(j)}, Y_{(k)}} \\ & \leq nL(X_{(j)}, Y_{(k)}) \left(1 + \frac{\alpha_0 \sqrt{\log \log n}}{\sqrt{n(1 - X_{(j)})(1 - Y_{(k)})}}\right) \\ & \leq nL\left(\frac{j}{n}, \frac{k}{n}\right) \left(1 + \frac{2\alpha_0 \sqrt{\log \log n}}{\log n}\right)^3 \end{aligned}$$

Therefore,

$$\begin{aligned} & n_{X_{(\pi(j))}, Y_{(\pi(k))}} \\ & \geq nL(X_{(\pi(j))}, Y_{(\pi(k))}) \left(1 - \frac{\alpha_0 \sqrt{\log \log n}}{\sqrt{n(1 - X_{(\pi(j))})(1 - Y_{(\pi(k))})}}\right) \\ & \geq nL\left(\frac{\pi(j)}{n}, \frac{\pi(k)}{n}\right) \left(1 - \frac{2\alpha_0 \sqrt{\log \log n}}{\log n}\right)^3 \\ & \geq nL\left(\frac{j}{n}, \frac{k}{n}\right) \left(1 - \frac{2\alpha_0 \sqrt{\log \log n}}{\log n}\right)^3 \left(1 + \frac{\sqrt{\log \log n}}{\log n}\right)^{-2} \end{aligned}$$

This implies

$$n_{X_{(j)}, Y_{(k)}} \leq n_{X_{(\pi(j))}, Y_{(\pi(k))}} \left(1 + \frac{20\alpha_0 \sqrt{\log \log n}}{\log n}\right), \quad (12)$$

for sufficiently large n . We then appeal to the following technical result.

Lemma 1. *Let X and Y be two independent uniform random variables. For two fixed pairs (t_X, t_Y) and (t'_X, t'_Y) , denote by*

$$B = \{n_{(\min(t_X, t'_X), \min(t_Y, t'_Y))} \leq (1+\epsilon)n_{(\max(t_X, t'_X), \max(t_Y, t'_Y))}\}.$$

Then

$$\mathbb{P}(|\tilde{\tau}(t_X, t_Y) - \tilde{\tau}(t'_X, t'_Y)| > r | B) \leq 4 \exp\left(-\frac{r^2}{72\epsilon^2 + 18\epsilon}\right), \quad (13)$$

where $\tilde{\tau}(t_X, t_Y)$ is defined in (10). In particular, if $\epsilon \leq 1/12$, we have

$$\mathbb{P}(|\tilde{\tau}(t_X, t_Y) - \tilde{\tau}(t'_X, t'_Y)| > r | B) \leq 4 \exp\left(-\frac{r^2}{24\epsilon}\right).$$

Lemma 1 immediately suggests that

$$\begin{aligned} & \mathbb{P}(|\tilde{\tau}(X_{(j)}, Y_{(k)}) - \tilde{\tau}(X_{(\pi(j))}, Y_{(\pi(k))})| > r) \\ & \leq 4 \exp\left(-\frac{r^2 \log n}{480\alpha_0 \sqrt{\log \log n}}\right). \end{aligned}$$

Because there are at most n^2 pairs (j, k) and $\log^4 n$ pairs $(\pi(j), \pi(k))$, an application of union bound yields

$$\mathbb{P}(|\tau_{\mathcal{N}_n}^* - \tau_2^*| > r) \leq 4n^2 \log^4 n \exp\left(-\frac{r^2 \log n}{480\alpha_0 \sqrt{\log \log n}}\right).$$

Taking $r = 2\sqrt{480\alpha_0} \log^{1/4} \log n$ yields

$$\mathbb{P}\left(|\tau_{\mathcal{N}_n}^* - \tau_2^*| > 2\sqrt{480\alpha_0} \log^{1/4} \log n\right) \rightarrow 0. \quad (14)$$

On the other hand, to bound $\tau_{\mathcal{N}_n}^*$, we now appeal to the following lemma.

Lemma 2. *If X and Y are independent uniform random variables, then*

$$\mathbb{P}(\tilde{\tau}(t_X, t_Y) > r | n_{t_X, t_Y} \geq 2) \leq \exp\left(-\frac{r^2}{9}\right), \quad (15)$$

where $\tilde{\tau}(t_X, t_Y)$ is defined in (10).

An application of union bounds and Lemma 2 yields

$$\begin{aligned} \mathbb{P}(\tau_{\mathcal{N}_n}^* > r) &\leq \log^4 n \sup_{(j,k) \in \mathcal{N}_n} \mathbb{P}(\tilde{\tau}(X_{(j)}, Y_{(k)}) > r) \\ &\leq \log^4 n \sup_{j,k} \mathbb{P}(\tilde{\tau}(X_{(j)}, Y_{(k)}) > r) \\ &\leq \log^4 n \sup_{j,k} \mathbb{P}(\tilde{\tau}(X_{(j)}, Y_{(k)}) > r | n_{X_{(j)}, Y_{(k)}} \geq 2) \\ &\leq \log^4 n \exp\left(-\frac{r^2}{9}\right) \end{aligned}$$

Taking $r = 7\sqrt{\log \log n}$ leads to

$$\mathbb{P}(\tau_{\mathcal{N}_n}^* > 7\sqrt{\log \log n}) \rightarrow 0. \quad (16)$$

Combined with (14) and (16), we obtain

$$\mathbb{P}(\tau_2^* > 8\sqrt{\log \log n}) \rightarrow 0.$$

Finally, we consider τ_3^* , which turns out to be the most complex. We first group (j, k) according to its size by defining the following collection of coordinates:

$$\mathcal{T}_n(M_i, \eta_i) = \{(j, k) : M_i/\eta_i \leq n(1-j/n)(1-k/n) \leq M_i\},$$

where $1 \leq i \leq Q_n$. Here, Q_n is the smallest integer such that $M_{Q_n+1} < \alpha_0^2 \log \log n$, and η_i and M_i be two positive sequences such that

$$M_1 = \log^2 n, \quad \eta_i = 1 + \frac{\sqrt{\log \log n}}{\sqrt{M_i}} \quad \text{and} \quad M_{i+1} = M_i/\eta_i.$$

It is not hard to see that

$$\tau_3^* = \max_{1 \leq i \leq Q_n} \max_{(j,k) \in \mathcal{T}_n(M_i, \eta_i)} \tilde{\tau}(X_{(j)}, Y_{(k)}).$$

We employ a strategy similar to the previous case to bound $\max_{(j,k) \in \mathcal{T}_n(M_i, \eta_i)} \tilde{\tau}(X_{(j)}, Y_{(k)})$ for each i . To this end, we define the following approximation set to $\mathcal{T}_n(M_i, \eta_i)$:

$$\begin{aligned} \mathcal{S}_n(M_i, \eta_i) &= \{(j, k) : (j, k) \text{ or } (k, j) \text{ is of form} \\ &\quad ([n - n/2\eta_i^u], [n - 2M_i\eta_i^{u+1}]), u = 0, \dots, \lfloor \frac{\log n}{2 \log \eta_i} \rfloor\}. \end{aligned}$$

We first bound to the difference between max on $\mathcal{S}_n(M_i, \eta_i)$ and on $\mathcal{T}_n(M_i, \eta_i)$. Similar to before, we consider a class of maps $\pi_i : \mathcal{T}_n(M_i, \eta_i) \rightarrow \mathcal{S}_n(M_i, \eta_i)$ such that

$$\pi_i(j, k) = \begin{cases} \left(\lfloor [n - n/2\eta_i^{h(j)}], [n - 2M_i\eta_i^{h(j)+1}] \right) & \text{if } j > k \\ \left(\lfloor [n - 2M_i\eta_i^{h(k)+1}], [n - n/2\eta_i^{h(k)}] \right) & \text{if } j \leq k \end{cases}$$

where $h(t)$ maps t to the largest u such that $\lfloor [n - n/2\eta_i^u] \rfloor < t$. For any $(j, k) \in \mathcal{S}_n(M_i, \eta_i)$, its pre-image $\pi_i^{-1}(j, k)$ is the collection of all pairs (j', k') in $\mathcal{T}_n(M_i, \eta_i)$ which satisfy $\pi_i(j', k') = (j, k)$. Moreover, we define a conjugate pair of $(j, k) \in \mathcal{S}_n(M_i, \eta_i)$ as

$$c(j, k) = \begin{cases} ([n - n/2\eta_i^{u+1}], [n - 2M_i\eta_i^u]) & \text{if } j > k \\ ([n - 2M_i\eta_i^u], [n - n/2\eta_i^{u+1}]) & \text{if } j \leq k \end{cases}$$

if u is an integer such that (j, k) or $(k, j) = ([n - n/2\eta_i^u], [n - 2M_i\eta_i^{u+1}])$. For simplicity, denote by $c(j, k)_x$ and $c(j, k)_y$ the two indices of $c(j, k)$. Figure 8 gives a specific example to illustrate the idea behind π_i , $\pi_i^{-1}(j, k)$ and conjugate pair $c(j, k)$.

As shown in Figure 8, for any $(j, k) \in \mathcal{S}_n(M_i, \eta_i)$,

$$\bigcup_{(j', k') \in \pi_i^{-1}(j, k)} \mathcal{K}(X_{(j')}, Y_{(k')}) \subset \mathcal{K}(X_{(j)}, Y_{(k)}),$$

where, recall that $\mathcal{K}(t_X, t_Y) = \{i \in \mathbb{I} : X_i \geq t_X, Y_i \geq t_Y\}$. This suggests that

$$\begin{aligned} &|\{\tilde{\tau}(X_{(j')}, Y_{(k')}) : (j', k') \in \pi_i^{-1}(j, k)\}| \\ &\leq \left(n_{X_{(j)}, Y_{(k)}} - n_{X_{(c(j,k)_x)}, Y_{(c(j,k)_y)}}\right)^2. \end{aligned} \quad (17)$$

Here $|\cdot|$ represents the cardinality of a set. By a similar argument as that for (12), we have

$$n_{X_{(j)}, Y_{(k)}} \leq n_{X_{(c(j,k)_x)}, Y_{(c(j,k)_y)}} \left(1 + \frac{20\alpha_0 \sqrt{\log \log n}}{\sqrt{M_i}}\right), \quad (18)$$

for any $(j, k) \in \mathcal{S}_n(M_i, \eta_i)$.

Equations (17) and (18) together imply that

$$\begin{aligned} &|\{\tilde{\tau}(X_{(j')}, Y_{(k')}) : (j', k') \in \pi_i^{-1}(j, k)\}| \\ &\leq (20\alpha_0 n_{X_{(j)}, Y_{(k)}} \sqrt{\log \log n} / \sqrt{M_i})^2 \\ &\leq \log^3 n. \end{aligned}$$

This means that the number of distinct values among $\{\tilde{\tau}(X_{(j')}, Y_{(k')}) : (j', k') \in \pi_i^{-1}(j, k)\}$ is not very large. We can then apply union bound, (18) and Lemma 1 to get

$$\begin{aligned} &\mathbb{P}\left(\left|\max_{(j,k) \in \mathcal{T}_n(M_i, \eta_i)} \tilde{\tau}(X_{(j)}, Y_{(k)}) - \max_{(j,k) \in \mathcal{S}_n(M_i, \eta_i)} \tilde{\tau}(X_{(j)}, Y_{(k)})\right| > r\right) \\ &\leq \sum_{(j,k) \in \mathcal{S}_n(M_i, \eta_i)} \mathbb{P}\left(\max_{(j', k') \in \pi_i^{-1}(j, k)} |\tilde{\tau}(X_{(j)}, Y_{(k)}) - \tilde{\tau}(X_{(j')}, Y_{(k')})| > r\right) \\ &\leq \sum_{(j,k) \in \mathcal{S}_n(M_i, \eta_i)} 4 \log^3 n \exp\left(-\frac{r^2}{24(\eta_i - 1)}\right) \\ &\leq 4 \log^5 n \exp\left(-\frac{r^2}{24(\eta_i - 1)}\right). \end{aligned}$$

Recall that

$$Q_n \leq T_1 \leq \log^2 n \quad \text{and} \quad \eta_i \leq 1 + \frac{1}{\alpha_0}.$$

Therefore,

$$\begin{aligned} & \mathbb{P} \left(\left| \max_{(j,k) \in \cup_{i=1}^{Q_n} \mathcal{T}_n(M_i, \eta_i)} \tilde{\tau}(X_{(j)}, Y_{(k)}) - \max_{(j,k) \in \cup_{i=1}^{Q_n} \mathcal{S}_n(M_i, \eta_i)} \tilde{\tau}(X_{(j)}, Y_{(k)}) \right| > r \right) \leq \log^4 n \exp \left(-\frac{r^2}{9} \right) \\ & \leq \sum_{i=1}^{Q_n} \mathbb{P} \left(\left| \max_{(j,k) \in \mathcal{T}_n(M_i, \eta_i)} \tilde{\tau}(X_{(j)}, Y_{(k)}) - \max_{(j,k) \in \mathcal{S}_n(M_i, \eta_i)} \tilde{\tau}(X_{(j)}, Y_{(k)}) \right| > r \right) \\ & \leq 4 \log^7 n \exp \left(-\frac{\alpha_0 r^2}{24} \right) \end{aligned} \quad (19)$$

It is clear that

$$\begin{aligned} & \left\{ (j, k) : j, k \geq \lfloor n/2 \rfloor, \frac{\alpha_0^2 \log \log n}{n} \leq L \left(\frac{j}{n}, \frac{k}{n} \right) \leq \frac{\log^2 n}{n} \right\} \\ & \subset \bigcup_{i=1}^{Q_n} \mathcal{T}_n(M_i, \eta_i) \end{aligned}$$

Taking $r = 16\sqrt{\log \log n}/\alpha_0$ in (19) yields

$$\mathbb{P} \left(\left| \tau_3^* - \max_{(j,k) \in \cup_{i=1}^{Q_n} \mathcal{S}_n(M_i, \eta_i)} \tilde{\tau}(X_{(j)}, Y_{(k)}) \right| > \frac{16\sqrt{\log \log n}}{\alpha_0} \right) \rightarrow 0 \quad (20)$$

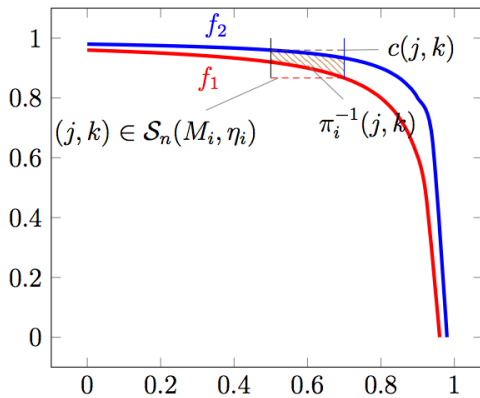


Fig. 8: $f_1 : n(1 - j/n)(1 - k/n) = M_i$ and $f_2 : n(1 - j/n)(1 - k/n) = M_i/\eta_i$, The shaded area is $\pi_i^{-1}(j, k)$ for some $(j, k) \in \mathcal{S}_n(M_i, \eta_i)$.

An application of union bound and Lemma 2 then yields

$$\begin{aligned} & \mathbb{P} \left(\max_{(j,k) \in \cup_{i=1}^{Q_n} \mathcal{S}_n(M_i, \eta_i)} \tilde{\tau}(X_{(j)}, Y_{(k)}) > r \right) \\ & \leq \sum_{i=1}^{Q_n} \mathbb{P} \left(\max_{(j,k) \in \mathcal{S}_n(M_i, \eta_i)} \tilde{\tau}(X_{(j)}, Y_{(k)}) > r \right) \\ & \leq \log^4 n \sup_{(j,k) \in \cup_{i=1}^{Q_n} \mathcal{S}_n(M_i, \eta_i)} \mathbb{P}(\tilde{\tau}(X_{(j)}, Y_{(k)}) > r) \end{aligned}$$

Taking $r = 7\sqrt{\log \log n}$ yields

$$\mathbb{P} \left(\max_{(j,k) \in \cup_{i=1}^{Q_n} \mathcal{S}_n(M_i, \eta_i)} \tilde{\tau}(X_{(j)}, Y_{(k)}) > 7\sqrt{\log \log n} \right) \rightarrow 0 \quad (21)$$

Together with (20), it implies that

$$\mathbb{P} \left(\tau_3^* > 7\sqrt{\log \log n} + \frac{16\sqrt{\log \log n}}{\alpha_0} \right) \rightarrow 0.$$

and we can complete proof. The statement about q_α then follows from the bounds we derived for τ_1^* , τ_2^* and τ_3^* .

b) *Type II error:* To prove the first statement, it now suffices to show that under H_0 , if

$$V(t_X, t_Y) \cdot T^2(t_X, t_Y) \gg \frac{\log \log n}{n},$$

then $\tau^* \gg \sqrt{\log \log n}$.

Recall that $\mathcal{K} = \{i : X_i > t_X, Y_i > t_Y\}$, and

$$\mathbb{E}(\text{sign}(X_i - X_j) \text{sign}(Y_i - Y_j) | i, j \in \mathcal{K}) = T(t_X, t_Y).$$

This suggests that

$$\mathbb{E}(\tau(t_X, t_Y) \cdot W(n_{t_X, t_Y}) | n_{t_X, t_Y} = k) \geq \frac{3}{4} \sqrt{k} T(t_X, t_Y).$$

Here, $W(x) := \sqrt{\frac{9x(x-1)}{2(2x+5)}}$. Clearly, n_{t_X, t_Y} follows binomial distribution $n_{t_X, t_Y} \sim \text{Bin}(n, \theta)$, where $\theta = 1 + F(t_X, t_Y) - F_X(t_X) - F_Y(t_Y)$. It is easy to derive from Chernoff's bounds that

$$\mathbb{P} \left(\frac{n\theta}{2} < n_{t_X, t_Y} < \frac{3n\theta}{2} \right) \rightarrow 1.$$

This implies that

$$\mathbb{P} \left(\tau(t_X, t_Y) \cdot W(n_{t_X, t_Y}) > \sqrt{\frac{9}{32}} \sqrt{n\theta} T(t_X, t_Y) \right) \rightarrow 1.$$

and hence

$$\mathbb{P} \left(\tau(t_X, t_Y) \cdot W(n_{t_X, t_Y}) \gg \sqrt{\log \log n} \right) \rightarrow 1.$$

It follows that

$$\tau^* \geq \tau(t_X, t_Y) \cdot \sqrt{\frac{9n_{t_X, t_Y}(n_{t_X, t_Y} - 1)}{2(2n_{t_X, t_Y} + 5)}} \gg \sqrt{\log \log n},$$

with probability tending to one.

c) *Lower bound.*: To show that we can not detect a signal under the condition (4), we consider a special case where under the null, $F_0(x, y) = xy\mathbb{1}(0 \leq x \leq 1, 0 \leq y \leq 1)$; and under the alternative, the joint distribution comes from variants of Farlie-Gumbel-Morgenstern family so that its density can be given by

$$\begin{aligned} & \frac{f(U_j, \gamma_j)}{dF_{(U, \gamma)}(x, y)} \\ &= \frac{dF_{(U, \gamma)}(x, y)}{dxdy} \\ &= \begin{cases} 1 + \gamma \left(1 - 2 \left(\frac{x-U}{1-U}\right)\right) \left(1 - 2 \left(\frac{y-U}{1-U}\right)\right) & U \leq x, y \leq 1 \\ 1 & \text{otherwise} \end{cases}, \end{aligned}$$

where U and γ is some constant between 0 and 1.

Let (U_j, γ_j) be a sequence of pairs such that $U_j = 1 - 1/2^j$ and $\gamma_j(1 - U_j) = 2\sqrt{\log \log n}/\sqrt{n}$ and let $M_n = \lfloor \log n/4 \rfloor$. It is not hard to verify that $F_{(U_j, \gamma_j)}$ s satisfy (4) with $c = 16/81$ by noting

$$V(U_j, U_j) \cdot T^2(U_j, U_j) = \frac{4\gamma_j^2}{81}(1 - U_j)^2.$$

Denote by \mathbb{P}_0 the joint distribution of $(X_i, Y_i)_{i=1}^n$ with distribution $F_0(x, y)$ and, for $j = 1, \dots, M_n$, \mathbb{P}_j joint distribution of $(X_i, Y_i)_{i=1}^n$ with density distribution of $F_{(U_j, \gamma_j)}(x, y)$. Then, the likelihood ratio between \mathbb{P}_j and \mathbb{P}_0 is

$$L_j := \frac{d\mathbb{P}_j}{d\mathbb{P}_0} = \prod_{i=1}^n f_{(U_j, \gamma_j)}(X_i, Y_i).$$

Elementary calculations lead to

$$\begin{aligned} & \mathbb{E}_0(f_{(U_j, \gamma_j)}(X_i, Y_i)f_{(U_k, \gamma_k)}(X_i, Y_i)) \\ &= 1 + \frac{\gamma_j(1 - U_j)\gamma_k(1 - U_k)}{9 * 2^{3|j-k|}} \\ &= 1 + \frac{4 \log \log n}{9n * 2^{3|j-k|}}, \end{aligned} \quad (22)$$

where \mathbb{E}_0 stands for expectation taken with respect to \mathbb{P}_0 . By definition and (22), we can ensure

$$\begin{aligned} \mathbb{E}_0(L_j L_k) - 1 &= \prod_{i=1}^n \mathbb{E}_0(f_{(U_j, \gamma_j)}(X_i, Y_i)f_{(U_k, \gamma_k)}(X_i, Y_i)) - 1 \\ &= \left(1 + \frac{4 \log \log n}{9n * 2^{3|j-k|}}\right)^n - 1 \\ &\leq \frac{1}{2^{3|j-k|}} \left(\left(1 + \frac{4 \log \log n}{9n}\right)^n - 1 \right) \\ &\leq \frac{1}{2^{3|j-k|}} \left(\exp\left(\frac{4 \log \log n}{9}\right) - 1 \right). \end{aligned}$$

This immediately suggests that

$$\sum_{j, k=1}^{M_n} (\mathbb{E}_0(L_j L_k) - 1) \leq 2M_n \exp\left(\frac{4 \log \log n}{9}\right).$$

Then, by Jensen's inequality, we have

$$\begin{aligned} & \mathbb{E}_0 \left(\left| \frac{1}{M_n} \sum_{j=1}^{M_n} L_j - 1 \right|^2 \right) \\ & \leq \mathbb{E}_0 \left(\left| \frac{1}{M_n} \sum_{j=1}^{M_n} L_j - 1 \right|^2 \right) \\ & \leq 2M_n^{-1} \exp\left(\frac{4 \log \log n}{9}\right) \rightarrow 0 \end{aligned} \quad (23)$$

Let ϕ be any test that depends on $\{X_i, Y_i\}_{i=1}^n$. Then, by (23),

$$\begin{aligned} & \max_{j=1, \dots, M_n} \mathbb{P}_j(\phi = 0) + \mathbb{P}_0(\phi = 1) \\ &= 1 - \min_{j=1, \dots, M_n} \mathbb{E}_j \phi + \mathbb{E}_0(\phi) \\ &\geq 1 - \frac{1}{M_n} \sum_{j=1}^{M_n} \mathbb{E}_j \phi + \mathbb{E}_0 \phi \\ &= 1 - \mathbb{E}_0 \left(\frac{1}{M_n} \sum_{j=1}^{M_n} L_j - 1 \right) \phi \\ &\geq 1 - \mathbb{E}_0 \left| \frac{1}{M_n} \sum_{j=1}^{M_n} L_j - 1 \right| \\ &\rightarrow 1 \end{aligned}$$

Here \mathbb{E}_j stands for expectation taken with respect to \mathbb{P}_j ; we complete the proof.

APPENDIX

PROOF OF TECHNICAL LEMMAS

Proof of Lemma 1. First consider a simple case where $(t_X - t'_X)(t'_Y - t_Y) = 0$ and assume $t_X = t'_X$ and $t_Y \leq t'_Y$ without loss of generality. Let $S = \{(t, s) : t_X \leq t \leq 1, t_Y \leq s \leq 1\}$ and $S' = \{(t, s) : t_X \leq t \leq 1, t'_Y \leq s \leq 1\}$. We randomly choose points $(\tilde{X}_i, \tilde{Y}_i)_{i=1}^{k'}$ in S' and points $(\tilde{X}_i, \tilde{Y}_i)_{i=k'+1}^k$ in $S \setminus S'$, where $k \leq (1 + \epsilon)k'$. Condition on $\{n_{t_X, t_Y} = k, n_{t'_X, t'_Y} = k'\}$, $\tilde{\tau}(t_X, t_Y) - \tilde{\tau}(t'_X, t'_Y)$ has the same distribution as the following statistic:

$$\begin{aligned} & f((\tilde{X}_i, \tilde{Y}_i)_{i=1}^k) \\ &= \frac{3\sqrt{2}}{\sqrt{k(k-1)(2k+5)}} \sum_{1 \leq i < j \leq k} \text{sign}(\tilde{X}_i - \tilde{X}_j) \text{sign}(\tilde{Y}_i - \tilde{Y}_j) \\ & - \frac{3\sqrt{2}}{\sqrt{k'(k'-1)(2k'+5)}} \sum_{1 \leq i < j \leq k'} \text{sign}(\tilde{X}_i - \tilde{X}_j) \text{sign}(\tilde{Y}_i - \tilde{Y}_j) \end{aligned}$$

Next, we show that f has bounded difference with respect to $(\tilde{X}_i, \tilde{Y}_i)$. Write

$$\begin{aligned} \Delta_j &:= \sup_{(\tilde{X}_i, \tilde{Y}_i)_{i=1}^k, (\tilde{X}'_j, \tilde{Y}'_j)} |f((\tilde{X}_i, \tilde{Y}_i)_{1 \leq i \leq k}) \\ & - f((\tilde{X}_i, \tilde{Y}_i)_{1 \leq i \leq k, i \neq j}, (\tilde{X}'_j, \tilde{Y}'_j))| \end{aligned}$$

When $1 \leq j \leq k'$,

$$\Delta_j \leq 3 \left(\frac{1}{\sqrt{k'}} - \frac{k'}{k\sqrt{k}} + \frac{k-k'}{k\sqrt{k}} \right) \leq \frac{6(k-k')}{k\sqrt{k'}}$$

and, when $k' < j \leq k$,

$$\Delta_j \leq \frac{3k'}{k\sqrt{k}}.$$

Because $k \leq (1 + \epsilon)k'$, we have

$$v = \frac{1}{4} \sum_j \Delta_j^2 \leq \frac{9(k - k')^2}{k^2} + \frac{9(k - k')}{4k} \leq 9\epsilon^2 + \frac{9}{4}\epsilon$$

Applying McDiarmid inequality [see, e.g., 27] to f ,

$$\begin{aligned} & \mathbb{P}(\tilde{\tau}(t_X, t_Y) - \tilde{\tau}(t'_X, t'_Y) > r | n_{t_X, t_Y} = k, n_{t'_X, t'_Y} = k') \\ & \leq \exp\left(-\frac{r^2}{18\epsilon^2 + 9\epsilon/2}\right) \end{aligned}$$

where we used the fact that $\mathbb{E}(f((\tilde{X}_i, \tilde{Y}_i)_{i=1}^k)) = 0$. By symmetry,

$$\begin{aligned} & \mathbb{P}(|\tilde{\tau}(t_X, t_Y) - \tilde{\tau}(t'_X, t'_Y)| > r | B) \\ & \leq 2\mathbb{P}(\tilde{\tau}(t_X, t_Y) - \tilde{\tau}(t'_X, t'_Y) > r | B) \\ & \leq 2 \exp\left(-\frac{r^2}{18\epsilon^2 + 9\epsilon/2}\right). \end{aligned}$$

Next, we consider the case when $t_X > t'_X$ and $t'_Y > t_Y$ and all other remaining cases can be treated in an identical fashion. Applying the result for $(t_X - t'_X)(t'_Y - t_Y) = 0$, we can derive that

$$\begin{aligned} & \mathbb{P}(|\tilde{\tau}(t_X, t_Y) - \tilde{\tau}(t'_X, t'_Y)| > r | B) \\ & \leq \mathbb{P}(|\tilde{\tau}(t_X, t_Y) - \tilde{\tau}(t_X, t'_Y)| > r/2 | B) \\ & \quad + \mathbb{P}(|\tilde{\tau}(t_X, t'_Y) - \tilde{\tau}(t'_X, t'_Y)| > r/2 | B) \\ & \leq 4 \exp\left(-\frac{r^2}{72\epsilon^2 + 18\epsilon}\right). \end{aligned}$$

This completes the proof. \square

Proof of Lemma 2. Note that

$$\begin{aligned} & \mathbb{P}(\tilde{\tau}(t_X, t_Y) > r | n_{t_X, t_Y} \geq 2) \\ & = \frac{\sum_{k=2}^n \mathbb{P}(\tilde{\tau}(t_X, t_Y) > r | n_{t_X, t_Y} = k) \mathbb{P}(n_{t_X, t_Y} = k)}{\mathbb{P}(n_{t_X, t_Y} \geq 2)} \\ & \leq \sup_{k \geq 2} \mathbb{P}(\tilde{\tau}(t_X, t_Y) > r | n_{t_X, t_Y} = k) \end{aligned}$$

Thus it is sufficient to set an upper bound to $\mathbb{P}(\tilde{\tau}(t_X, t_Y) > r | n_{t_X, t_Y} = k)$. Condition on $n_{t_X, t_Y} = k$, $\tilde{\tau}(t_X, t_Y)$ has the same distribution with

$$\frac{3\sqrt{2}}{\sqrt{k(k-1)(2k+5)}} \sum_{1 \leq i < j \leq k} \text{sign}(\tilde{X}_i - \tilde{X}_j) \text{sign}(\tilde{Y}_i - \tilde{Y}_j)$$

where $(\tilde{X}_i, \tilde{Y}_i)_{i=1}^k$ comes from distribution given $X > t_X$ and $Y > t_Y$. Using the concentration inequality for U-statistics from [28], we get

$$\begin{aligned} & \mathbb{P}(\tilde{\tau}(t_X, t_Y) - \mathbb{E}(\tilde{\tau}(t_X, t_Y)) | n_{t_X, t_Y} = k) > r | n_{t_X, t_Y} = k) \\ & \leq e^{-r^2/9}. \end{aligned}$$

The proof is then completed noting that \tilde{X}_i and \tilde{Y}_i remain independent of each other. \square

REFERENCES

- [1] S. Bolte and F. P. Cordelières, “A guided tour into subcellular colocalization analysis in light microscopy,” *Journal of Microscopy*, vol. 224, no. 3, pp. 213–232, 2006.
- [2] J. Comeau, S. Costantino, and P. Wiseman, “A guide to accurate fluorescence microscopy colocalization measurements,” *Biophysical Journal*, vol. 91, no. 12, pp. 4611–4622, 2006.
- [3] E. Manders, J. Stap, G. Brakenhoff, R. V. Driel, and J. Aten, “Dynamics of three-dimensional replication patterns during the s-phase, analysed by double labelling of dna and confocal microscopy,” *Journal of Cell Science*, vol. 103, no. 3, pp. 857–862, 1992.
- [4] E. Manders, F. Verbeek, and J. Aten, “Measurement of co-localization of objects in dual-colour confocal images,” *Journal of Microscopy*, vol. 169, no. 3, pp. 375–382, 1993.
- [5] S. Costes, D. Daelemans, E. Cho, Z. Dobbin, G. Pavlakakis, and S. Lockett, “Automatic and quantitative measurement of protein-protein colocalization in live cells,” *Biophysical Journal*, vol. 86, no. 6, pp. 3993–4003, 2004.
- [6] Y. Wu, M. Eghbali, J. Ou, R. Lu, L. Toro, and E. Stefani, “Quantitative determination of spatial protein-protein correlations in fluorescence confocal microscopy,” *Biophysical Journal*, vol. 98, no. 3, pp. 493–504, 2010.
- [7] K. W. Dunn, M. M. Kamocka, and J. H. McDonald, “A practical guide to evaluating colocalization in biological microscopy,” *American Journal of Physiology-Cell Physiology*, vol. 300, no. 4, pp. 723–742, 2011.
- [8] J. Adler, S. Pagakis, and I. Parmryd, “Replicate-based noise corrected correlation for accurate measurements of colocalization,” *Journal of microscopy*, vol. 230, no. 1, pp. 121–133, 2008.
- [9] A. French, S. Mills, R. Swarup, M. Bennett, and T. Pridmore, “Colocalization of fluorescent markers in confocal microscope images of plant cells,” *Nature protocols*, vol. 3, no. 4, p. 619, 2008.
- [10] V. Zinchuk, Y. Wu, O. Grossenbacher-Zinchuk, and E. Stefani, “Quantifying spatial correlations of fluorescent markers using enhanced background reduction with protein proximity index and correlation coefficient estimations,” *Nature Protocols*, vol. 6, no. 10, pp. 1554–1567, 2011.
- [11] B. Dengler, *On the asymptotic behaviour of the estimator of Kendall’s Tau*. Ph.D. Thesis, 2010.
- [12] P. Embrechts, A. McNeil, and D. Straumann, “Correlation and dependence in risk management: properties and pitfalls,” *Risk management: value at risk and beyond*, 2002.
- [13] E. L. Lehmann, “Some concepts of dependence,” *Ann. Math. Statist.*, vol. 37, no. 5, pp. 1137–1153, 1966.
- [14] R. B. Nelsen, *An introduction to copulas*. New York: Springer, 2006.
- [15] E. Arias-Castro, D. Donoho, and X. Huo, “Near-optimal detection of geometric objects by fast multiscale methods,” *IEEE Transactions on Information Theory*, vol. 51,

- no. 7, pp. 2402–2425, 2005.
- [16] G. Walther, “Optimal and fast detection of spatial clusters with scan statistics,” *The Annals of Statistics*, vol. 38, no. 2, pp. 1010–1033, 2010.
- [17] H. Chan and G. Walther, “Detection with the scan and the average likelihood ratio,” *Statistica Sinica*, vol. 23, pp. 409–428, 2013.
- [18] C. Rivera and G. Walther, “Optimal detection of a jump in the intensity of a poisson process or in a density with likelihood ratio statistics,” *Scandinavian Journal of Statistics*, vol. 40, no. 4, pp. 752–769, 2013.
- [19] S. Wang, J. Fan, G. Pocock, and M. Yuan, “Structured correlation detection with application to colocalization analysis in dual-channel fluorescence microscopic imaging,” *arXiv preprint arXiv:1604.02158*, 2016.
- [20] E. Freed, “Hiv-1 assembly, release and maturation,” *Nature Reviews. Microbiology*, vol. 13, no. 8, p. 484, 2015.
- [21] W. Sundquist and H. Kräusslich, “Hiv-1 assembly, budding, and maturation,” *Cold Spring Harbor perspectives in medicine*, vol. 2, no. 7, p. a006924, 2012.
- [22] J. Becker and N. Sherer, “Subcellular localization of hiv-1 gag-pol mrnas regulates sites of virion assembly,” *Journal of virology*, vol. 91, no. 6, pp. e02315–16, 2017.
- [23] C. Simon, E. Vaughan, W. Bement, and L. Edelstein-Keshet, “Pattern formation of rho gtpases in single cell wound healing,” *Molecular biology of the cell*, vol. 24, no. 3, pp. 421–432, 2013.
- [24] E. Vaughan, J. You, H. Yu, A. Lasek, N. Vitale, T. Hornberger, and W. Bement, “Lipid domain-dependent regulation of single-cell wound repair,” *Molecular biology of the cell*, vol. 25, no. 12, pp. 1867–1876, 2014.
- [25] E. Arena, C. Rueden, M. Hiner, S. Wang, M. Yuan, and K. W. Eliceiri, “Quantitating the cell: turning images into numbers with imagej,” *Wiley Interdisciplinary Reviews: Developmental Biology*, 2016.
- [26] J. H. J. Einmahl, “Extension to higher dimensions of the jaeschke-eicker result on the standardized empirical process,” *Communications in Statistics-Theory and Methods*, vol. 25, no. 4, pp. 813–822, 1996.
- [27] S. Boucheron, G. Lugosi, and P. Massart, *Concentration inequalities: A nonasymptotic theory of independence*. New York: Oxford University Press, 2013.
- [28] W. Hoeffding, “Probability inequalities for sums of bounded random variables,” *Journal of the American statistical association*, vol. 58, no. 301, pp. 13–30, 1963.